Supplement of Solid Earth, 12, 141–170, 2021
https://doi.org/10.5194/se-12-141-2021-supplement

Solid Earth
Open Access

Supplement of

Distribution, microphysical properties, and tectonic controls of deformation bands in the Miocene subduction wedge (Whakataki Formation) of the Hikurangi subduction zone

Kathryn E. Elphick et al.

Correspondence to: Kathryn E. Elphick (elphickk@qut.edu.au)

Supplement Section S.1

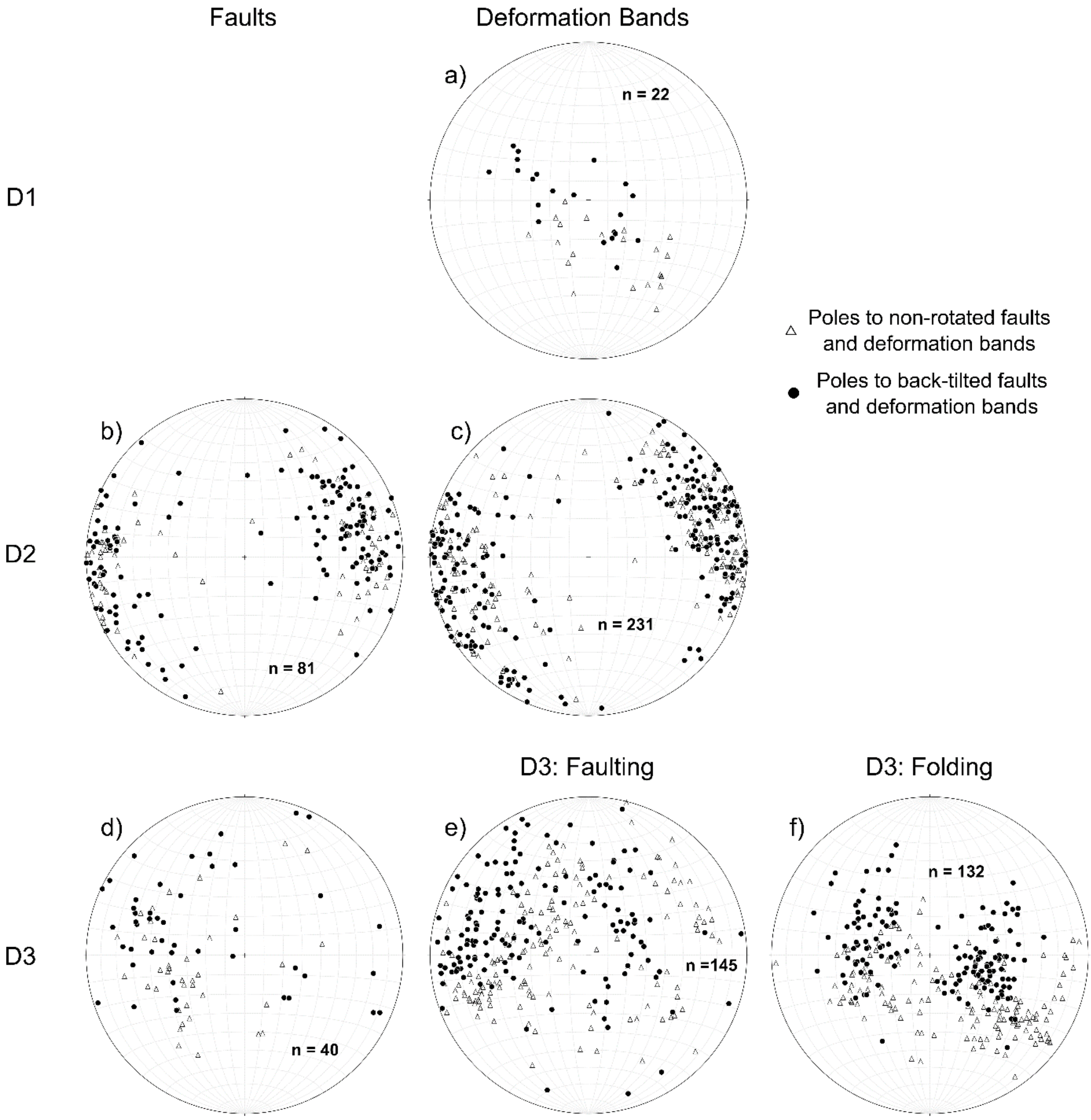

Figure S1. Schmidt nets of back-tilted orientations of structural features compared with present-day orientations. Structural data was back-tilted using the nearest S_0 measurement in Stereonet 10 (Allmendinger et al., 2011). a) Deformation bands associated with D1 faulting. b) Normal faults formed during D2 horizontal extension. c) Deformation bands with normal-sense shear formed during D2 horizontal extension. d) Reverse faults formed during D3 horizontal contraction. e) Deformation bands with reverse-sense shear formed during D3 horizontal contraction. f) Deformation bands with a regular spacing and minimal offset observed in areas of folded sandstone beds, formed during D3 horizontal contraction. Tight clustering of these bands when in their original orientation indicates that they have since been rotated with folding.

Supplement Section S.2

Table S1. Table of microfabric data for analysed thin sections.

	Sample	Band width (mm)	Host rock average perimeter (um)	DB average perimeter (um)	HR diameter (um)	DB Diameter (um)	Aspect ratio (HR)	Aspect ratio (DB)	Grainsize Reduction (%)	Band offset (mm)	DB porosity	DB porosity fraction	HR Porosity	HR porosity fraction
D2 FDZ	48.1	0.636	171.65	59.39	54.64	18.90	1.63	1.68	35%	4.40	7.30	0.07	13.50	0.13
	97.4	1.505	257.44	147.21	81.95	46.86	1.50	1.63	57%	6.20	4.93	0.05	12.66	0.13
	97.1.2	1.300	195.57	157.03	62.25	49.98	1.58	1.61	80%	8.30	2.89	0.03	9.83	0.10
	131.5	0.877	283.55	161.85	90.26	51.52	1.55	1.58	57%	5.60	8.49	0.08	17.43	0.17
	74.3	0.917	216.14	65.17	68.80	20.75	1.62	1.60	30%	6.10	7.96	0.08	18.71	0.19
	53.3.2	0.939	213.39	56.61	67.92	18.02	1.76	1.14	27%	5.50	8.08	0.08	17.17	0.17
	53.1.2	0.807	143.51	86.23	45.68	27.45	1.65	1.58	60%	4.80	7.04	0.07	13.19	0.13
	53.1.1	0.952	258.45	61.45	82.27	19.56	1.58	1.63	24%	6.10	5.55	0.06	14.12	0.14
	53.3.1	0.742	245.68	74.61	78.20	23.75	1.67	1.65	30%	6.20	8.93	0.09	16.71	0.17
	101.1	0.827	254.32	115.02	80.95	36.61	1.62	1.69	45%	3.20	6.04	0.06	19.09	0.19
D3 FDZ	141.1.2	1.830	217.33	84.30	69.18	26.83	1.71	1.66	39%	11.20	12.03	0.12	26.09	0.26
	74.5	0.639	178.99	44.62	56.97	14.20	1.53	1.68	25%	6.80	13.30	0.13	21.19	0.21
	96.1	0.791	246.35	147.98	78.41	47.10	1.61	1.57	60%	3.80	12.53	0.13	19.20	0.19
	141.1	1.979	209.30	93.24	66.62	29.68	1.67	1.64	45%	5.60	11.15	0.11	16.57	0.17
	141.1.1	1.513	202.43	76.17	64.44	24.24	1.57	1.53	38%	6.20	13.48	0.13	18.08	0.18
D3 non-FDZ	1.1	1.002	157.36	92.49	50.09	29.44	1.71	1.69	59%	0.10	11.86	0.12	20.09	0.20
	3.1	0.581	173.15	104.68	55.12	33.32	1.68	1.64	60%	0.02	8.63	0.09	16.01	0.16
	4.1	0.526	166.19	104.54	52.90	33.28	1.68	1.66	63%	0.08	8.71	0.09	20.01	0.20
	11.2	0.695	142.59	98.56	45.39	31.37	1.74	1.65	69%	0.15	6.03	0.06	17.88	0.18
	11.3	0.635	76.34	46.40	24.30	14.77	1.76	1.60	61%	0.02	5.16	0.05	17.24	0.17

	Sample	Weights	DB neg error	DB pos error	HR neg error	HR pos error	Dc	Ds/Dc	Dihedral angle	Porosity Reduction	Macro spacing (cm)	Damage zone width (cm)	Fault offset (cm)	Bed thickness (cm)	Location (lat)	Location (long)	Type of Band	Lithology (Facies)
D2 FDZ	48.1	0.19	1.33	1.36	2.10	2.13	0.05	96.59	N/A	6.20	NL	12.00	30.00	N/A	-40.938763	176.169680	Normal CSB	FA3
	97.4	0.23	1.13	1.13	1.62	1.64	0.13	46.56	N/A	7.73	NL	> 55 cm IDZ	195.00	N/A	-40.925111	176.190607	Normal CSB	FA2
	97.1.2	0.22	0.64	0.63	1.53	1.54	0.10	82.96	N/A	6.94	NL	> 55 cm IDZ	195.00	N/A	-40.925111	176.190607	Normal CSB	FA2
	131.5	0.22	1.82	1.84	2.49	2.55	0.09	59.01	N/A	8.94	NL	> 30 cm IDZ	55.00	N/A	-40.929451	176.181770	Normal CSB	FA2
	74.3	0.15	1.15	1.16	1.61	1.64	0.12	50.31	N/A	10.74	NL	4.00	31.00	N/A	-40.936817	176.173234	Normal CSB	FA2
	53.3.2	0.22	1.76	1.77	2.19	2.24	0.10	53.33	N/A	9.09	NL	> 200 cm IDZ	> 10 m	N/A	-40.938075	176.170602	Normal CSB	FA3
	53.1.2	0.17	1.18	1.18	2.06	2.08	0.06	83.95	N/A	6.15	NL	> 200 cm IDZ	> 10 m	N/A	-40.938075	176.170602	Normal CSB	FA3
	53.1.1	0.22	1.22	1.21	2.27	2.29	0.10	64.19	N/A	8.57	NL	> 200 cm IDZ	> 10 m	N/A	-40.938075	176.170602	Normal CSB	FA3
	53.3.1	0.12	0.99	1.03	1.96	1.89	0.07	89.48	N/A	7.78	NL	> 200 cm IDZ	> 10 m	N/A	-40.938075	176.170602	Normal CSB	FA3
	101.1	0.19	1.16	1.14	2.60	2.64	0.13	23.99	N/A	13.05	NL	0.10	4.00	N/A	-40.944526	176.160817	Normal CSB	FA3
D3 FDZ	141.1.2	0.25	2.99	3.01	2.62	2.72	0.35	32.16	N/A	14.06	NL	145.00	3.00	N/A	-40.941299	176.165649	Reverse CSB	FA3
	74.5	0.19	2.52	2.55	2.00	2.04	0.06	106.30	N/A	7.89	NL	6.00	12.00	N/A	-40.936817	176.173234	Reverse CSB	FA2
	96.1	0.17	2.07	2.10	2.19	2.24	0.07	58.18	N/A	6.67	NL	272.00	10.00	N/A	-40.930442	176.180182	Reverse CSB	FA2
	141.1	0.22	2.45	2.47	2.16	2.21	0.13	43.52	N/A	5.42	NL	145.00	3.00	N/A	-40.941299	176.165649	Reverse CSB	FA3
	141.1.1	0.18	2.37	2.42	1.82	1.87	0.09	72.92	N/A	4.60	NL	145.00	3.00	N/A	-40.941299	176.165649	Reverse CSB	FA3
D3 non-FDZ	1.1	0.16	1.87	1.91	1.49	1.52	0.10	0.97	88.00	8.24	11.80	N/A	N/A	80.10	-40.939025	176.168786	SECB	FA3
	3.1	0.14	1.21	1.22	1.51	1.52	0.05	0.39	76.00	7.38	6.80	N/A	N/A	40.90	-40.938891	176.169167	SECB	FA3
	4.1	0.19	1.63	1.65	1.66	1.70	0.07	1.08	75.00	11.30	2.20	N/A	N/A	29.20	-40.938865	176.169072	SECB	FA3
	11.2	0.16	0.97	0.98	1.31	1.33	0.10	1.50	68.00	11.85	30.00	N/A	N/A	93.80	-40.938841	176.169425	SECB	FA3
	11.3	0.15	0.76	0.77	1.25	1.27	0.09	0.22	68.00	12.08	30.00	N/A	N/A	93.80	-40.938813	176.169415	SECB	FA3

Key	FDZ	Fault Damage Zone
	IDZ	Interaction Damage Zone
	CSB	Compactional Shear Band
	SECB	Shear-Enhanced Compaction Band
	FA2	50:50 mudstone to sandstone
	FA3	Sandstone dominated
	HR	Host Rock
	DB	Deformation Band
	NL	Non-Linear

Supplement Section S.3

Table S2. Table of results from Pearson correlation coefficient analysis of deformation band spacing.

	Fault	Mean P	Median P	P Range	P IQR
D2 FDZ	Day 23 D2	0.10	0.07	0.62	0.06
	Day 24 D2	0.47	0.60	1.62	0.04
	Fault 14	0.15	0.10	1.19	0.06
	Fault 17.1	0.32	0.33	0.43	0.16
	Fault 17.2	0.62	0.61	0.25	0.04
	Fault 100	0.44	0.46	0.21	0.03
	Fault 161	0.42	0.42	0.62	0.07
D3 FDZ	Day 23 D3	-0.02	0.25	1.36	0.53
	Fault 96	0.13	0.17	1.65	0.10
	Fault 102	0.11	0.22	1.16	0.35
	Fault 117	0.67	0.59	0.43	0.22
	Fault 141	0.66	0.62	0.52	0.05
D3 non-FDZ	Bed 1 Set 2	-0.17	-0.07	0.95	0.04
	Bed 1 Set 1	-0.69	-0.64	0.40	0.09
	Bed 2 Set 2	0.03	-0.10	1.23	0.30
	Bed 3 Set 1	-0.25	-0.27	0.94	0.20
	Bed 4 Set 2	0.09	0.25	1.48	0.59
	Bed 6 Set 1	0.02	0.04	1.11	0.04
	Bed 7 Set 1	-0.15	-0.07	1.17	0.13
	Bed 8 Set 1	0.31	0.32	0.90	0.20
	Bed 9.2 Set 1	0.34	0.34	0.71	0.31
	Bed 10 Set 1	0.42	0.39	0.27	0.17
	Bed 10 Set 1 Main	0.42	0.40	0.32	0.31
	Bed 10 Set 2	0.29	0.31	0.84	0.06
	Bed 11 Set 2	-0.31	-0.32	1.82	0.24
	S1 B1 set 2	-0.39	-0.29	0.81	0.34
	S1 B2 set 1	0.31	0.33	1.50	0.14
	S1 B3 set 1	0.04	0.04	1.49	0.19
	S2 B2 set 1	0.57	0.61	1.68	0.04
	S2 B3 set 1	0.09	0.10	1.21	0.23
	S3 B3 set 2	-0.40	-0.32	0.92	0.60
	Stop 2	-0.73	-0.65	0.63	0.42
	Stop 3	0.37	0.16	1.09	0.90
	Stop 4 bed 1	-0.12	-0.07	0.99	0.08
	Stop 4 bed 2	-0.15	-0.13	1.03	0.09
	Stop 4 bed 3	-0.17	-0.25	1.16	0.12
	Stop 5	0.09	0.13	0.99	0.08
	Stop 6	0.32	0.32	0.60	0.03
	Stop 7	0.21	0.10	0.96	0.13
	Stop 8	-0.27	-0.25	0.89	0.06

Key	FDZ	Fault Damage Zone
	IQR	Inter-QuartileRange
	P	Pearson Correlation Coefficient

Supplement Section S.4

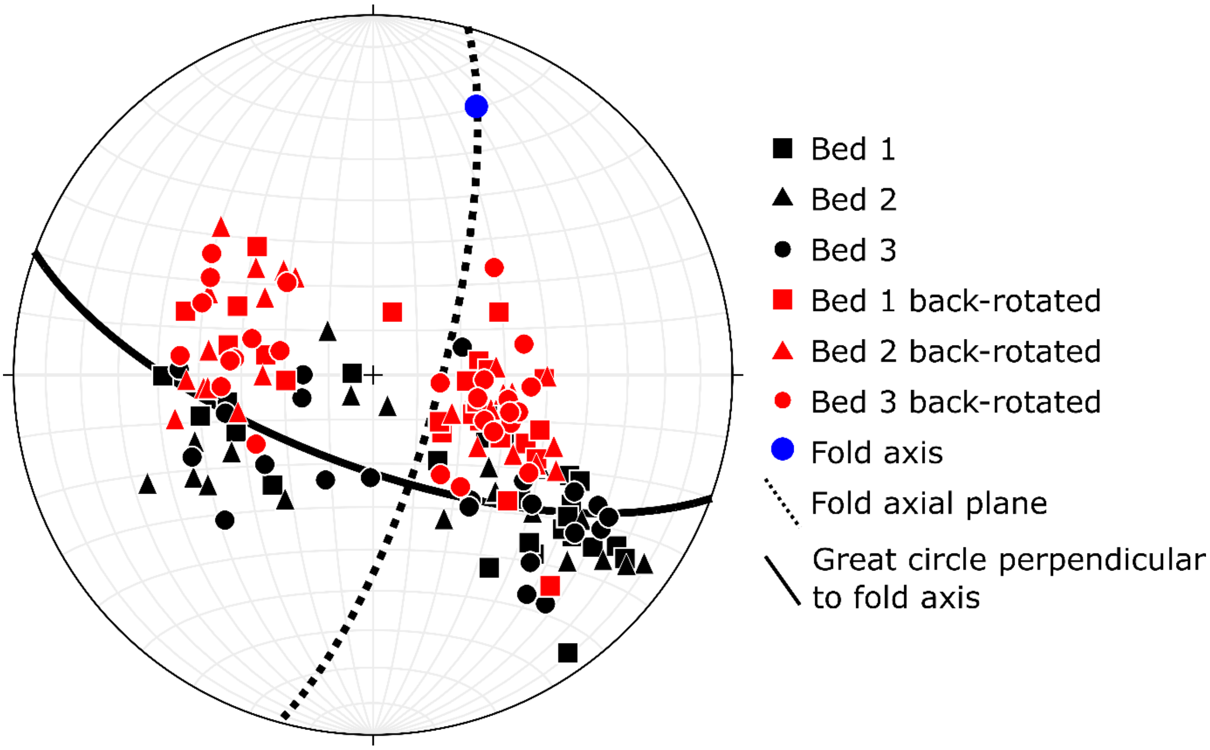

Figure S2. Schmidt net showing the orientations of deformation bands in three beds across a fold hinge. Deformation band present day orientation, and back-rotated orientations are shown. Present data orientation aligns with the great circle that is perpendicular to the fold axis indicating that deformation bands have been passively rotated with the folding of the host beds.

Supplement Section S.5

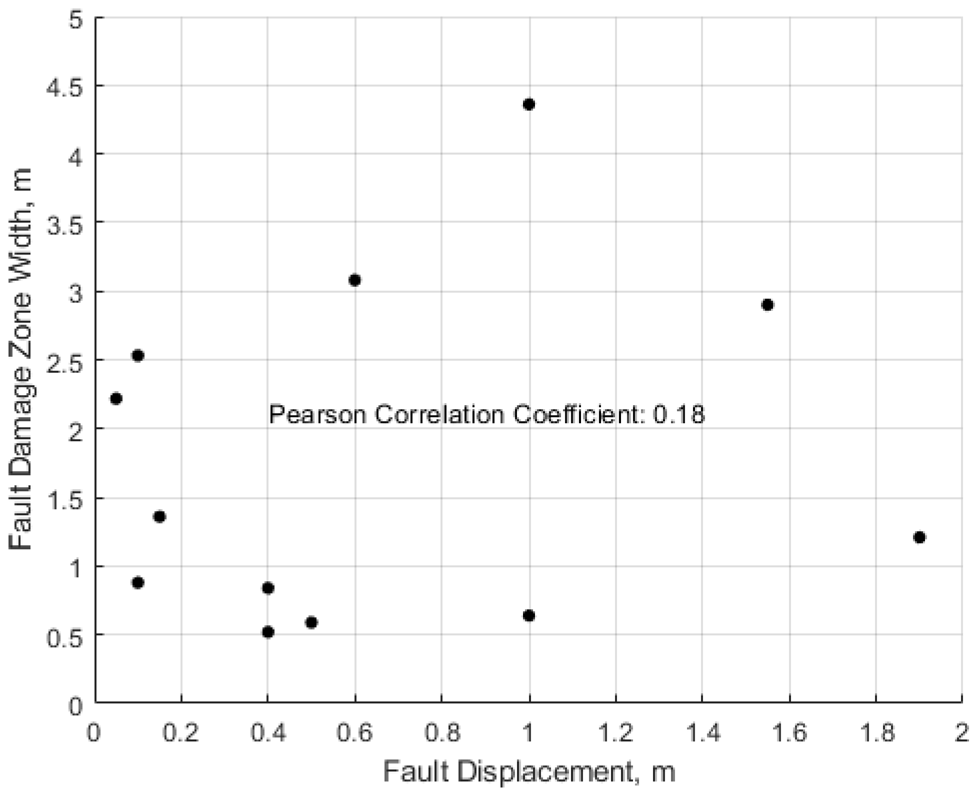

Figure S3. A plot to show the relationship between the fault displacement and the associated damage zone width. Fault displacement was measured where true displacement could be calculated from slip vector orientations and the separation of sedimentary markers across the fault plane (Shipton et al., 2006). Data shows that there is no correlation between the width of a damage zone and the offset of the associated fault.

Supplement Section S.6

Table S3. Table to show estimated permeability values. Equation used to estimate permeability from porosity: $\ln k = 21.41 + 11.425\, ln\phi_e + 1.327(ln\phi_e)^2$ (Wu, 2004). Order of magnitude reduction (OoMR) was calculated using: $OoMR = log_{10}\frac{Host\ Rock\ Permeability}{Deformation\ Band\ Permeability}$

	Porosity (%)	**Permeability (mD)**	**Order of magnitude reduction**
D2 Host Rock	13.00	38.00	1.98
D2 Deformation Band	5.00	0.40	
D3 FDZ Host Rock	20.00	645.00	1.45
D3 FDZ Deformation Band	12.00	23.00	
D3 non-FDZ Host Rock	19.00	449.00	1.95
D3 non-FDZ Deformation Band	9.00	5.00	

Supplement Section S.7

Table S4. Table to show the correlation statistics from porosity analysis of different band kinematics shown in Figure 9.

Porosity Analysis	Band Kinematics	Pearson	R^2
Host Rock and Deformation Band	*D2 CSB, D3 CSB, SECB*	0.69	0.47
	D2 CSB	0.72	0.51
	D3 CSB	0.06	0.00
	SECB	0.56	0.32
Host Rock and Absolute Porosity Reduction	*D2 CSB, D3 CSB, SECB*	0.55	0.30
	D2 CSB	0.79	0.62
	D3 CSB	0.97	0.94
	SECB	0.14	0.02

Supplement Section S.8

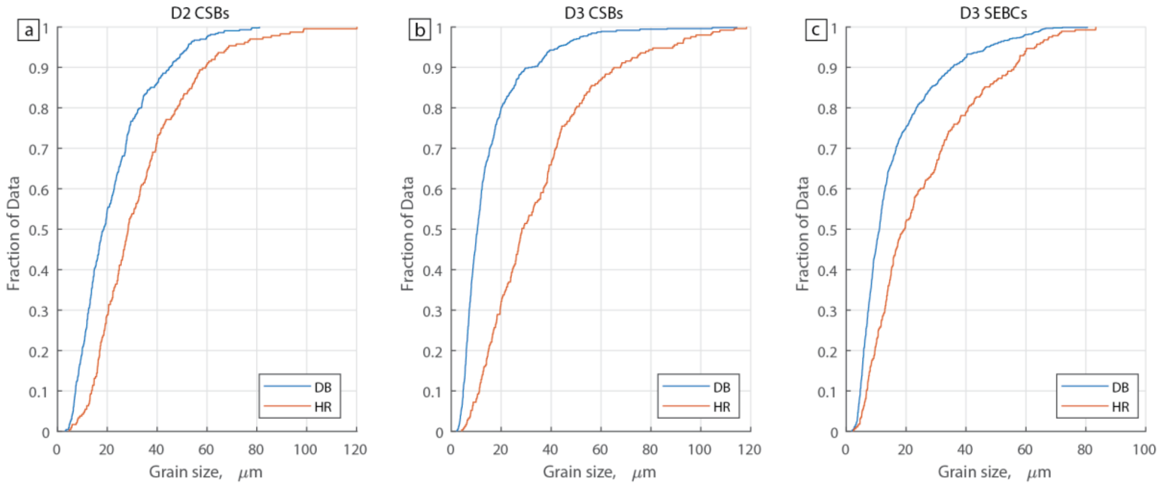

Figure S4. Empirical cumulative distribution plots to show the variation in grain sizes measured in thin sections of D2 CSBs [a], D3 CSBs [b], and D3 SECBs [c]. Two-sample Kolmogorov-Smirnov tests indicate that for each type of DB, the difference between the grain size within the DB and within the adjacent host rock is statistically significant. Within each DB, the grain size reduces.

Supplement Section S.9

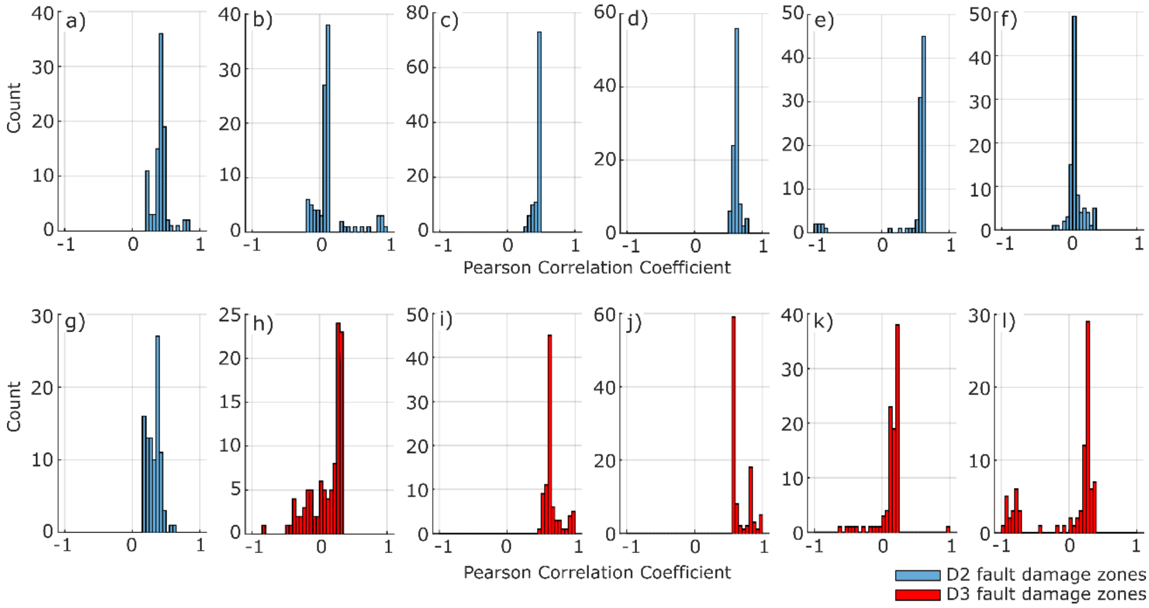

Figure S5. Histograms to show Pearson correlation coefficient values established from multiple scan-lines along deformation band maps from fault damage zones (FDZs). D2 FDZ and D3 FDZ are differentiated by colour. Many analyses have a main peak ca. 0.5 indicating a positive relationship between the spacing of deformation bands and the distance of those bands from a fault plane. However, within the dataset, there are peaks at values that are closer to 0. E.g.: in b) where the peak value is ca. 0.1 or h) where there is a cluster of peaks around 0. Peaks that have Pearson values that are close to zero indicate that there is no relationship between spacing and distance from the fault plane and is indicative of regular spacing. The range in Pearson values for each outcrop indicates that the spacing between deformation bands and the distance from a fault plane are not described by a simple relationship and that this relationship can vary on the outcrop scale.

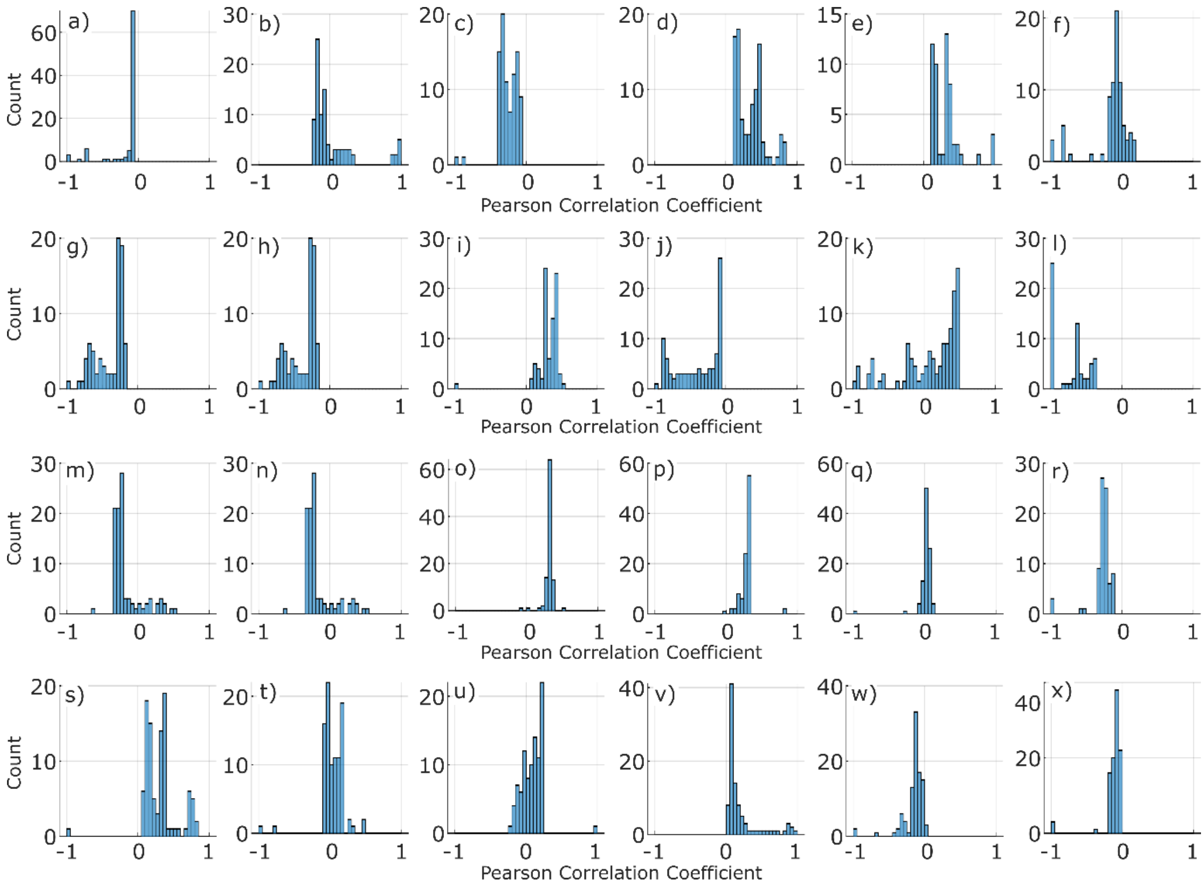

Figure S6. Histograms to show Pearson correlation coefficient values for D3 deformation bands that are characterised by minimal offset and a regular spacing (D3 non-FDZ). The spacing of bands has been compared to the distance perpendicular to strike. Most histograms show a peak ca. 0. This indicates no relationship between spacing and distance. There are, however, instances of a large spread of Pearson data e.g. in image (k). 12 out of 28 outcrops analysed have a spread of Pearson data that is greater than 1. This indicates that there can be scan-lines across a single outcrop that are identifying band populations with positive, negative, and zero correlation between the spacing and distance from the image origin.

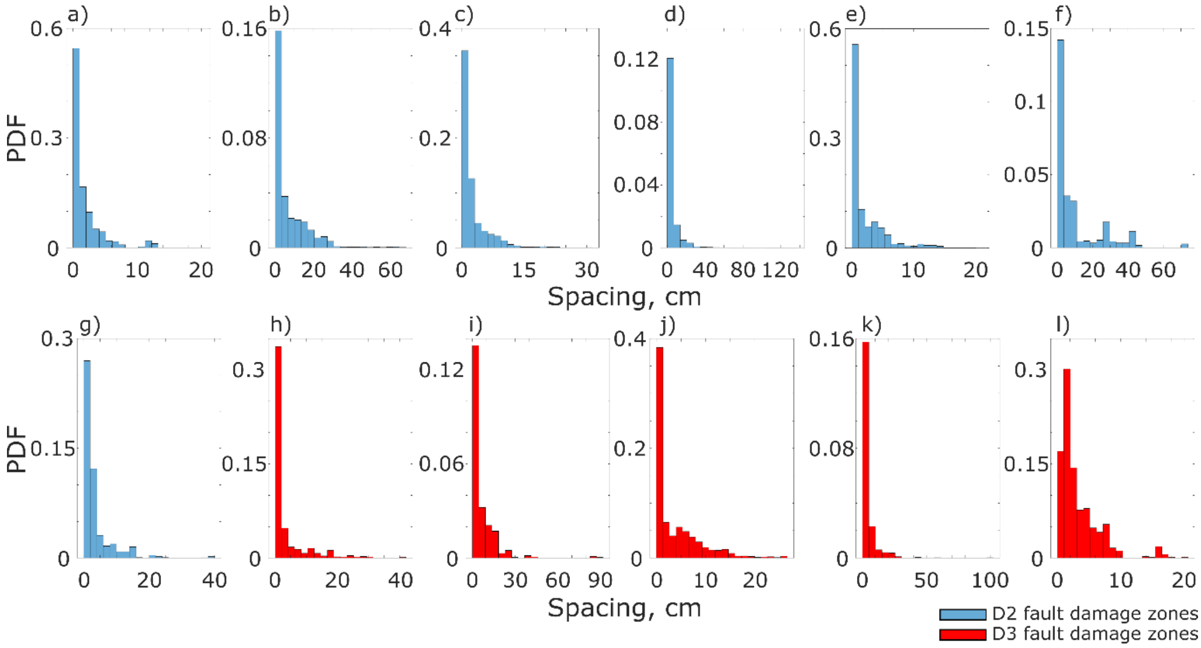

Figure S7. Histograms to show the frequency distribution of absolute spacing measurements between bands in fault damage zones. The probability density function is on the y-axis. The histograms have a positive skew representing the decay of damage away from the fault plane.

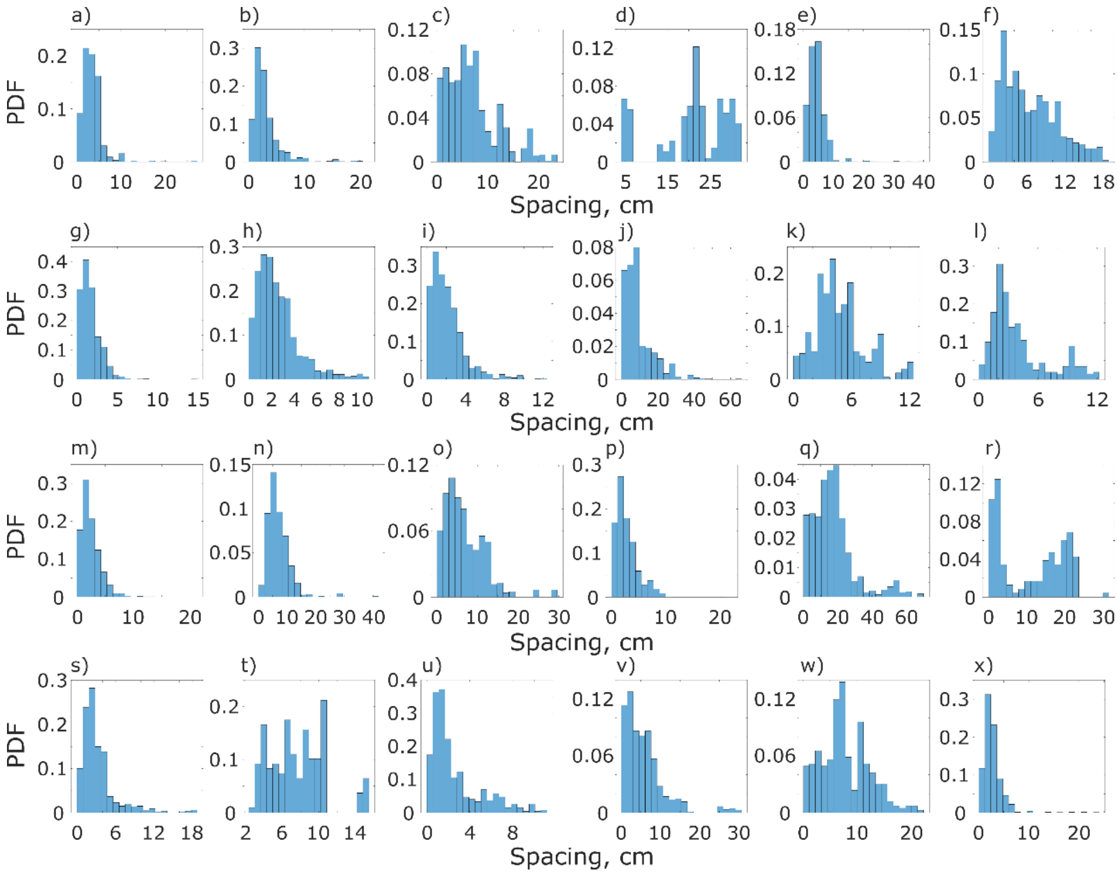

Figure S8. Histograms to show the probability density function of spacing of D3 deformation bands observed in outcrops that are not directly adjacent to a fault. In these outcrops, deformation bands show a 'regular' spacing. The bands analysed in this plot are characterised by minimal offset / no observable offset. Histogram plots are not consistent. Some have a bimodal distribution (e.g. d and l). Some are characterised by a normal distribution (e.g., k and t). Many have a positive skew yet compared to 'fault-associated' band spacing, there is a broader spread, indicative of regularly spaced bands, with noise (Fig. S10b).

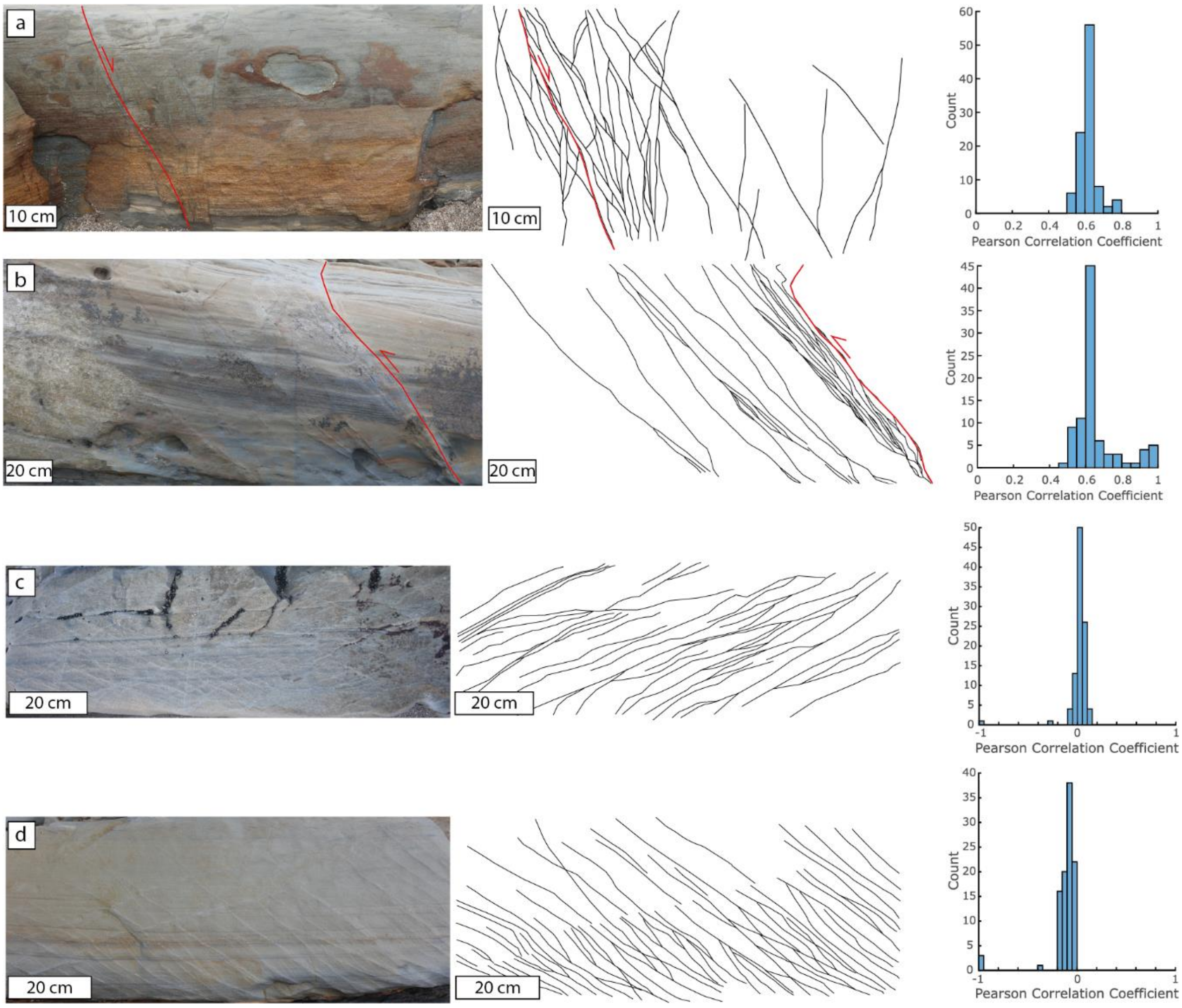

Figure S9. [a], [b] Spacing analysis of CSBs associated with the damage zone of faults. 100 scan-lines were taken for each image during analysis. [a] represents a D2 normal fault and [b] shows a small D3 reverse fault. Both faults show an increase in spacing between deformation bands with increasing distance from the fault plane. This is reflected in the Pearson correlation coefficient. Values are approaching 1, which shows a dependence of distance on spacing. [c], [d] Spacing analysis of dominantly SECBs with rare CSBs not associated with the damage zone of faults. 100 scan-lines were taken for each image during analysis. Each image shows a general lack of correlation of the distance with the spacing between deformation bands. Pearson correlation coefficient values close to 0 further suggest a lack of correlation. These bands show a near-constant spacing. Median spacing: [c] = 1.8 cm; and [d] = 2.3 cm.

Supplement Section S.10

In this research, we have created six synthetic images to show ideal spacing distributions and to highlight how natural variation in heterogeneous rocks and data collection errors can impact the measured spacing of natural sample. These images are created as an interpretive guide to analyse natural spacing distributions. The six synthetic images represent (Fig. S10):

[a] Deformation bands with constant spacing

[b] Deformation bands with constant spacing and added noise to replicate measuring bias and outcrop conditions. The noise in image [b] was generated by adding an array of random values, between 0 and 0.8 of the constant spacing value, to the space. The random values are collectively characterised by a normal distribution and a median value of 0

[c] Deformation bands spatially characterised by an exponential spatial decay away from a fault

[d] Deformation bands characterised by an exponential spatial decay away from a fault with integrated noise. Noise in the image [d] is generated by adding values up to 0.4 of the maxima spacing onto each spacing measurement, with added values collectively characterised by a normal distribution with a median value of 0

[e] Deformation band spacing that reflects the overprint of an equally spaced distribution [a] by an exponentially decaying damage zone [c]

[f] Deformation band spacing reflecting the overprint of an equal distribution with integrated noise [b] by an exponentially decaying damage zone also containing integrated noise [d].

Bands with a strictly constant spacing show a zero Pearson correlation coefficient (Fig. S10a). With the addition of normally distributed 'noise' to case [a], a distributed set of spacing with Gaussian noise is obtained (Fig. S10b). In this case [b], the Pearson correlation coefficient of spacing over distance is -0.08. The third synthetic image [c] represents a damage zone with an exponential decay of deformation band density away from the fault plane (Fig. S10c). For this example, the Pearson correlation coefficient between spacing and distance to the fault is exactly 1 (Fig. S10c). A histogram of this spacing distribution shows positive skew. The same results are expected for any other analytical expression in which spacing grows monotonously with distance from the fault (e.g., the power-law relationship established by Savage and Brodsky (2011)). With the addition of Gaussian noise to a damage zone [d], the Pearson correlation coefficient reduces to 0.56 (Fig. S10d). However, its exact value depends on the amount of noise and can be larger or smaller. Synthetic image [e] represents an overprint of two distributions, equal spacing and variable spacing, simulating two different deformation events affecting the same bed subsequently (Fig. S10e). If the deformation bands resulting from the two events are morphologically similar, they may be difficult to distinguish in the field and can be mapped together as one. In this case, the Pearson value is 0.71, although it could be any value between 0 and 1 dependent upon the value of spacing in the background density compared with the damage zone spacing. In image [f], noise is integrated into both distributions and they are combined (Fig. S10f). This is the most realistic outcome if there is an overprint of two events with different distributions. In the case shown, the Pearson value is 0.59. However, with different magnitudes of noise and varied initial spacings, any value from -1 to 1 could be obtained. For the interpretation of our field data, we assume a positive correlation between band spacing and spatial location if the Pearson value is > 0.5.

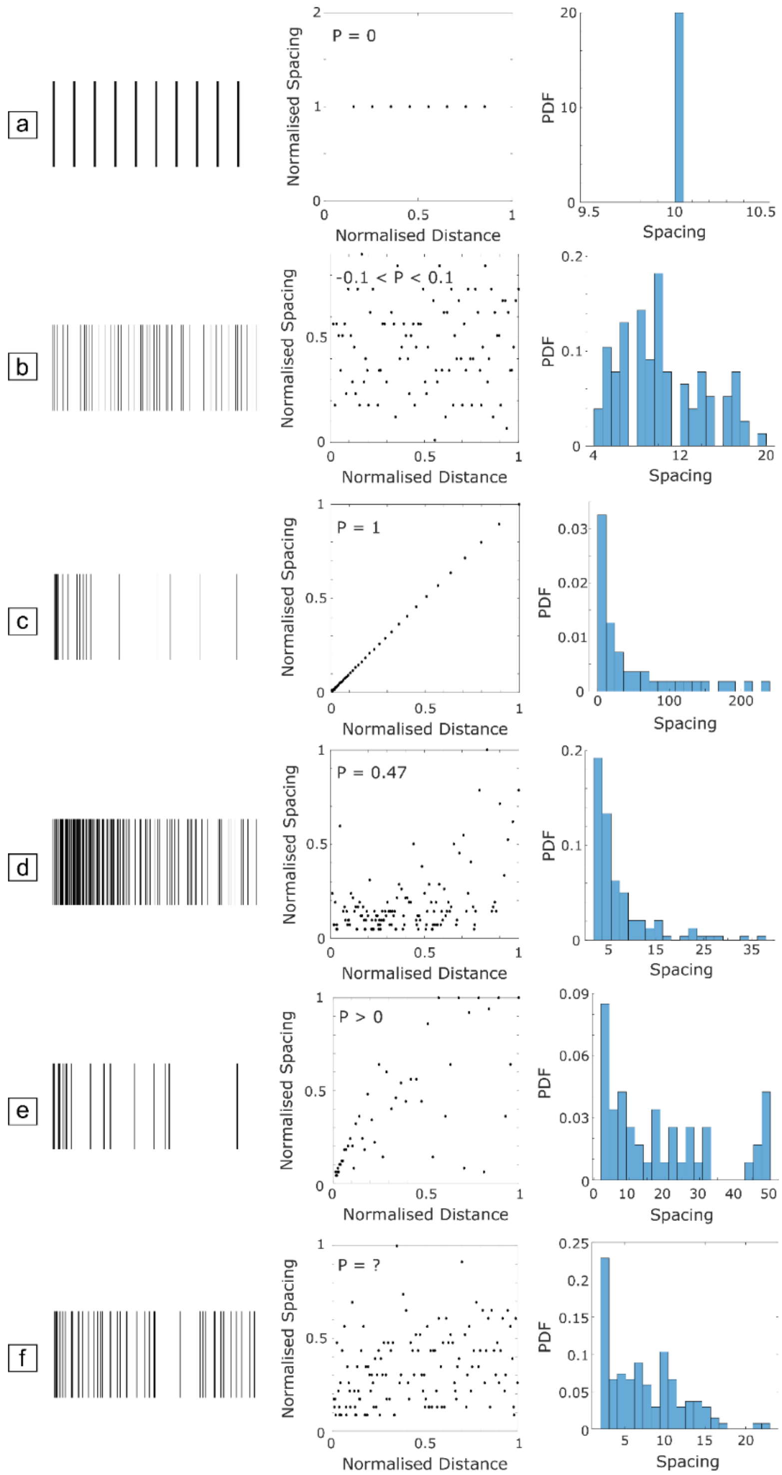

Figure S10. Synthetic images produced to replicate different distributions of the deformation bands. [a] deformation bands with a constant spacing, [b] deformation bands with a constant spacing with added Gaussian noise, [c] bands with an exponential decay away from a fault plane, and [d] deformation bands with an exponential decay away from a fault plane with added Gaussian noise. [e] and [f] represent images that combine constant spacing with a damage zone. These examples would be relevant if a damage zone overprinted a constant background spacing of the deformation band. [e] combines [a] with [c]. [f] combines [b] and [d] resulting in a spacing that contains two distributions that have noise. The relationship between spacing and distance is analysed using the Pearson correlation coefficient. Values close to 1 show a positive relationship between the distance from a point and the spacing. This would be seen in a damage zone that shows an increase in spacing between deformation bands as the distance from the fault plane increases. Pearson correlation coefficient values close to 0 show no correlation between spacing and distance. A histogram of the spacing is also shown. Unimodal distributions with no skew reflect bands with near-constant spacing. A positive skew represents damage zones. Distance and spacing are also plotted for different scan-lines. Distance is normalised to the maximum distance and spacing is normalised to the maximum spacing. P = Pearson correlation coefficient value.

References

Allmendinger, R. W., Cardozo, N., and Fisher, D. M.: Structural geology algorithms: Vectors and tensors, Cambridge University Press, 2011.

Savage, H. M. and Brodsky, E. E.: Collateral damage: Evolution with displacement of fracture distribution and secondary fault strands in fault damage zones, Journal of Geophysical Research, 116, 2011.

Shipton, Z., Soden, A., Kirkpatrick, J., Bright, A., and Lunn, R.: How Thick is a Fault? Fault Displacement-Thickness Scaling Revisited, Earthquakes: Radiated Energy and the Physics of Faulting, 170, 2006.

Wu, T.: Permeability prediction and drainage capillary pressure simulation in sandstone reservoirs., 2004. Texas A&M University, 2004.